AGU PUBLICATIONS

Geophysical Research Letters

RESEARCH LETTER
10.1002/2017GL075677

Circum-Antarctic Shoreward Heat Transport Derived From an Eddy- and Tide-Resolving Simulation

Andrew L. Stewart[1], **Andreas Klocker**[2,3,4], **and Dimitris Menemenlis**[5]

[1]Department of Atmospheric and Oceanic Sciences, University of California, Los Angeles, CA, USA, [2]Institute for Marine and Antarctic Studies, University of Tasmania, Hobart, Tasmania, Australia, [3]Australian Research Council Centre of Excellence for Climate System Science, University of Tasmania, Hobart, Tasmania, Australia, [4]Antarctic Climate and Ecosystems Cooperative Research Centre, University of Tasmania, Hobart, Tasmania, Australia, [5]Jet Propulsion Laboratory Science Division, California Institute of Technology, Pasadena, CA, USA

Key Points:
- Circum-Antarctic shoreward heat transport due to tides, eddies, and mean flows is quantified using a high-resolution ocean/sea ice model
- Eddies transport heat across the continental slope, while tides produce the largest shoreward heat flux across the shelf break
- Tidal heat fluxes are localized upstream of troughs in the continental shelf but are locally compensated by offshore mean heat fluxes

Supporting Information:
- Supporting Information S1

Correspondence to:
A. L. Stewart,
astewart@atmos.ucla.edu

Citation:
Stewart, A. L., Klocker, A., & Menemenlis, D. (2018). Circum-Antarctic shoreward heat transport derived from an eddy- and tide-resolving simulation. *Geophysical Research Letters*, *45*, 834–845. https://doi.org/10.1002/2017GL075677

Received 13 SEP 2017
Accepted 21 DEC 2017
Accepted article online 3 JAN 2018
Published online 19 JAN 2018

Abstract Almost all heat reaching the bases of Antarctica's ice shelves originates from warm Circumpolar Deep Water in the open Southern Ocean. This study quantifies the roles of mean and transient flows in transporting heat across almost the entire Antarctic continental slope and shelf using an ocean/sea ice model run at eddy- and tide-resolving (1/48°) horizontal resolution. Heat transfer by transient flows is approximately attributed to eddies and tides via a decomposition into time scales shorter than and longer than 1 day, respectively. It is shown that eddies transfer heat across the continental slope (ocean depths greater than 1,500 m), but tides produce a stronger shoreward heat flux across the shelf break (ocean depths between 500 m and 1,000 m). However, the tidal heat fluxes are approximately compensated by mean flows, leaving the eddy heat flux to balance the net shoreward heat transport. The eddy-driven cross-slope overturning circulation is too weak to account for the eddy heat flux. This suggests that isopycnal eddy stirring is the principal mechanism of shoreward heat transport around Antarctica, though likely modulated by tides and surface forcing.

1. Introduction

Oceanic heat transport toward Antarctica plays a significant role in the near-Antarctic and global climate systems. Basal melting of marine-terminating glaciers in West Antarctica has accelerated in recent decades (Jenkins et al., 2016) and has been projected to contribute substantially to sea level rise during the 21st century (DeConto & Pollard, 2016). There is also evidence that historically "cold" ice shelves may be melting (Silvano et al., 2017) or likely to experience rapid melt in coming decades (Hellmer et al., 2012, 2017). These changes may be felt globally via their impact on the thermodynamics of Antarctic Bottom Water (AABW) formation (Naveira Garabato et al., 2016), which ventilates a large fraction of the abyssal ocean and exerts substantial influence over large-scale ocean circulation and climate on millennial time scales (Ferrari et al., 2014; Orsi et al., 2001). In recent decades, AABW has globally exhibited thinning, warming, and freshening, likely related to processes occurring at its formation sites on the Antarctic shelf (Purkey & Johnson, 2013; Schmidtko et al., 2014).

Oceanic melting of the Antarctic ice sheet results predominantly from intrusions of Circumpolar Deep Water (CDW) (Rignot & Jacobs, 2002), a water mass that occupies the middepth ocean close to the Antarctic continent (Orsi et al., 1995) and to a lesser extent from warm summer surface waters (e.g., Arzeno et al., 2014; Zhou et al., 2014) and salty, near-freezing waters sourced from coastal polynyas (e.g., Nicholls et al., 2009). The Antarctic continental slope inhibits southward transport of CDW by geostrophic mean flows, instead supporting a sharp Antarctic Slope Front (ASF), coinciding with the westward Antarctic Slope Current (ASC), along most of the continental shelf break (see Figure 1; Jacobs, 1991; Whitworth et al., 1998). The along-slope geostrophic flows of the ASC and the Antarctic Coastal Current facilitate water mass transport between sectors of the Antarctic margins (e.g., Graham et al., 2013; Nakayama et al., 2014), but the strong cross-slope potential vorticity gradient implies that alternative physical mechanisms are necessary to support CDW transport across the ASF (Thompson et al., 2014).

Recent studies emphasize the role of small-scale processes, notably mesocale eddies and tides, in facilitating heat transfer across the continental shelf/slope. For example, while the Antarctic shelf has long been known

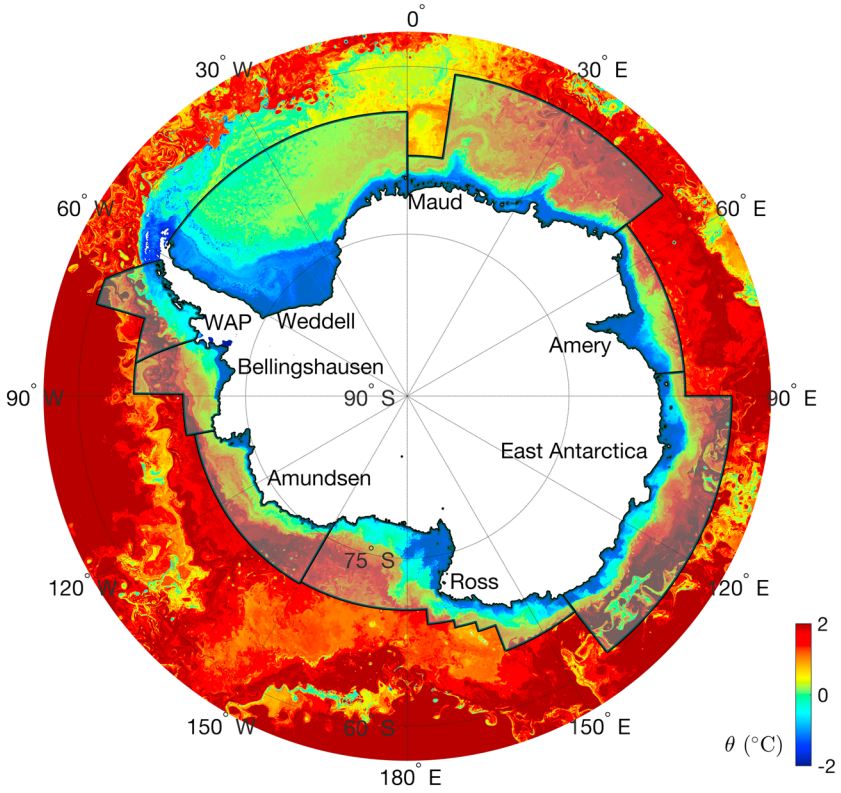

Figure 1. Snapshot of the LLC_4320 simulation, with overlays and labels indicating our regional division of the Antarctic margins. The colors correspond to potential temperature (θ) on simulation date 9 October 2012 at a depth of 230 m or at the ocean bed in regions shallower than 230 m.

to support relatively strong tidal ellipses and mixing (e.g., Foldvik et al., 1990; MacAyeal, 1984; Robertson, 2001), studies demonstrating that tidal fluctuations can substantially enhance cross-slope exchange have only materialized in the last decade (e.g., Mack et al., 2017; Padman et al., 2009; Wang et al., 2013). Mesoscale eddies can transfer CDW onto the shelf when isopycnals connect the shelf waters to the open ocean, for example, in regions where the ASF is absent (e.g., Couto et al., 2017; Graham et al., 2016; Martinson & Mckee, 2012; Nakayama et al., 2014) or where AABW descends the continental slope (e.g., Stewart & Thompson, 2015a; Thompson et al., 2014). Eddies can also support intrusions of CDW along the ocean bed in regions where there is a pronounced ASF (Hattermann et al., 2014; Nøst et al., 2011).

Despite the significance of the ASF for the near-Antarctic and global ocean circulation, our understanding of the dynamics underlying circum-Antarctic cross-slope exchanges lags far behind that of the broader Southern Ocean (Dinniman et al., 2016; Heywood et al., 2016). Taking in situ measurements near Antarctica is logistically difficult, though substantial advances have been made via campaigns like AnSlope (e.g., Gordon et al., 2004, 2009), and the small Rossby radius of deformation (Hallberg, 2013) requires models to use horizontal grid spacings on the order of 1 km in order to adequately resolve CDW transport by mesoscale eddies (St-Laurent et al., 2013; Stewart & Thompson, 2015b) and baroclinic tides (Padman et al., 2009). Previous modeling studies have therefore either focused on localized regions (e.g., Graham et al., 2016; Hattermann et al., 2014) or have employed coarser-resolution circum-Antarctic configurations with no representation of these small-scale processes (e.g., Dinniman et al., 2016; Schodlok et al., 2016). Consequently, the continental-scale transport of heat onto the Antarctic shelf remains poorly constrained. In this study we take a first look at circum-Antarctic shoreward heat fluxes due to high-frequency processes using an ocean/sea ice simulation run at 1/48° horizontal grid spacing that encompasses the entire Antarctic margins.

2. Model Description and Analysis

We derive estimates of shoreward heat transfer from a global ocean/sea ice simulation, which we refer to as LLC_4320. This simulation has been described previously (Rocha et al., 2016), but we discuss salient

properties of the model configuration here to achieve a self-contained presentation. Figure 1 illustrates the near-Antarctic portion of the simulation via a snapshot of potential temperature at 230 m depth or at the ocean bed where the bathymetry is shallower than 230 m. Further information about the model configuration is given in supporting information Text S1 (Arthern et al., 2006; Daru & Tenaud, 2004; Fox-Kemper & Menemenlis, 2008; Jackett & Mcdougall, 1995; Jourdain et al., 2017; Millan et al., 2017).

The LLC_4320 simulation was conducted using the Massachusetts Institute of Technology (MIT) general circulation model (Marshall, Hill, Perelman & Adcroft, 1997; Marshall, Adcroft, Hill, Perelman & Heisey, 1997) on a global Latitude-Longitude-Cap (LLC) grid (Forget et al., 2015) with 1/48° horizontal grid spacing and 90 vertical levels. The horizontal grid spacing is less than 1 km over the entire Antarctic continental shelf and slope, with the exception of the tip of the Antarctic Peninsula, which is sufficient to simulate shoreward heat transfer by eddies (Stewart & Thompson, 2015b; St-Laurent et al., 2013). The model includes the 16 largest-amplitude tidal components globally and partially resolves the internal wave spectrum (Rocha et al., 2016) and thus cross-slope excursions associated with baroclinic tides (Padman et al., 2009). The LLC_4320 simulation is not directly constrained by observational data but is a high-resolution continuation of the ECCO2 0.14° reanalysis product. The simulation spans September 2011 to October 2012 and derives surface fluxes from European Centre for Medium-Range Weather Forecasts 1/6° operational analysis (European Centre for Medium-Range Weather Forecasts, 2011) combined with an annual climatology of continental runoff (Fekete et al., 2002). An identically configured simulation was run using 1/24° horizontal grid spacing, spanning January 2011 to April 2013 and is referred to as LLC_2160. We reproduced all results derived from the LLC_4320 simulation using the LLC_2160 to evaluate the robustness of our findings and their sensitivity to the model grid spacing.

In the open ocean individual eddies have turnover time scales on the order of weeks to months (Smith & Vallis, 2001), so the duration of the LLC_4320 simulation would be too short to quantify eddy heat fluxes locally (Flierl & McWilliams, 1977). However, over the Antarctic continental slope the small (<5 km) Rossby radius results in an eddy turnover time on the order of days (e.g., Stewart & Thompson, 2016), which reduces the sampling duration required to achieve converged statistics. Temporal sampling issues can be offset via spatial averaging; for example, we compute cross-slope heat fluxes and model properties (Figures 2–4) using averages along sectors of the Antarctic continental slope. However, local estimates of statistical quantities like eddy kinetic energy (Figure 3) appear to be robust over the continental shelf and slope, exhibiting only small (10–20%) quantitative changes when the analysis is performed over 1 year (using LLC_4320) or 2 years (using LLC_2160; see supporting information Figures S5–S7).

A central aim of this paper is to determine the relative contributions of mean flows, eddies, and tides to shoreward heat transport. To perform this attribution, we decompose advective heat fluxes by exploiting the separation of time scales between these flows, posing a linear decomposition of the model output variables into mean, eddy, and tidal components. For example, the potential temperature θ is decomposed as

$$\theta = \theta_{\mathrm{m}} + \theta_{\mathrm{e}} + \theta_{\mathrm{t}}, \quad \theta_m = \overline{\theta}^{t,e}, \quad \theta_e = \overline{\theta}^{t} - \overline{\theta}^{t,e}, \quad \theta_t = \theta - \overline{\theta}^{t}, \tag{1}$$

where θ_m, θ_e, and θ_t denote the mean, eddy, and tidal components, respectively. We define $\overline{\bullet}^{t}$ as an average over each consecutive day and $\overline{\bullet}^{e}$ as an average over all of the days in the simulation. By definition the high-frequency tidal component vanishes under the short-time scale average, $\overline{\theta_{\mathrm{t}}}^{t} = 0$, and the lower-frequency eddy component vanishes under the long-time scale average, $\overline{\theta_{\mathrm{e}}}^{e} = 0$. This allows quadratic products, for example, the advective heat flux vector $\boldsymbol{F}_{\theta}$, to be decomposed into mean, eddy, and tidal components as well

$$\boldsymbol{F}_{\theta} = \boldsymbol{F}_{\mathrm{e}} + \boldsymbol{F}_{\mathrm{t}} + \boldsymbol{F}_{\mathrm{m}} = \overline{\boldsymbol{u}\theta}^{t,e}, \quad \boldsymbol{F}_{\mathrm{m}} = \overline{u}^{t,e}\overline{\theta}^{t,e}, \quad \boldsymbol{F}_{\mathrm{e}} = \overline{\boldsymbol{u}_{\mathrm{e}}\theta_{\mathrm{e}}}^{e}, \quad \boldsymbol{F}_{\mathrm{t}} = \overline{\boldsymbol{u}_{\mathrm{t}}\theta_{\mathrm{t}}}^{t,e}. \tag{2}$$

While this is a mathematically exact and conservative decomposition, it is not phenomenologically exact. For example, tidal cross-slope transport can vary substantially over each spring/neap cycle (e.g., Padman et al., 2009), while the "eddy" component includes all variability occurring on longer time scales, including seasonal variations and changes driven by atmospheric synoptic-scale variability. Additionally, diurnal variation in the ocean surface forcing will project onto the "tide" component. While nonlinear interaction between these phenomena precludes an exact decomposition (e.g., Ardhuin et al., 2017; Rocha et al., 2016), a closer approximation might be achieved using harmonic analysis to isolate the tidal variability (e.g., Foreman & Henry, 1989) and by separating the seasonal cycle from the eddies (e.g., Dufour et al., 2015). These approaches were found to be impractical due to the very large volume of model output, which is provided as hourly snapshots and occupies several petabytes of storage space; even simply time averaging the circum-Antarctic model output

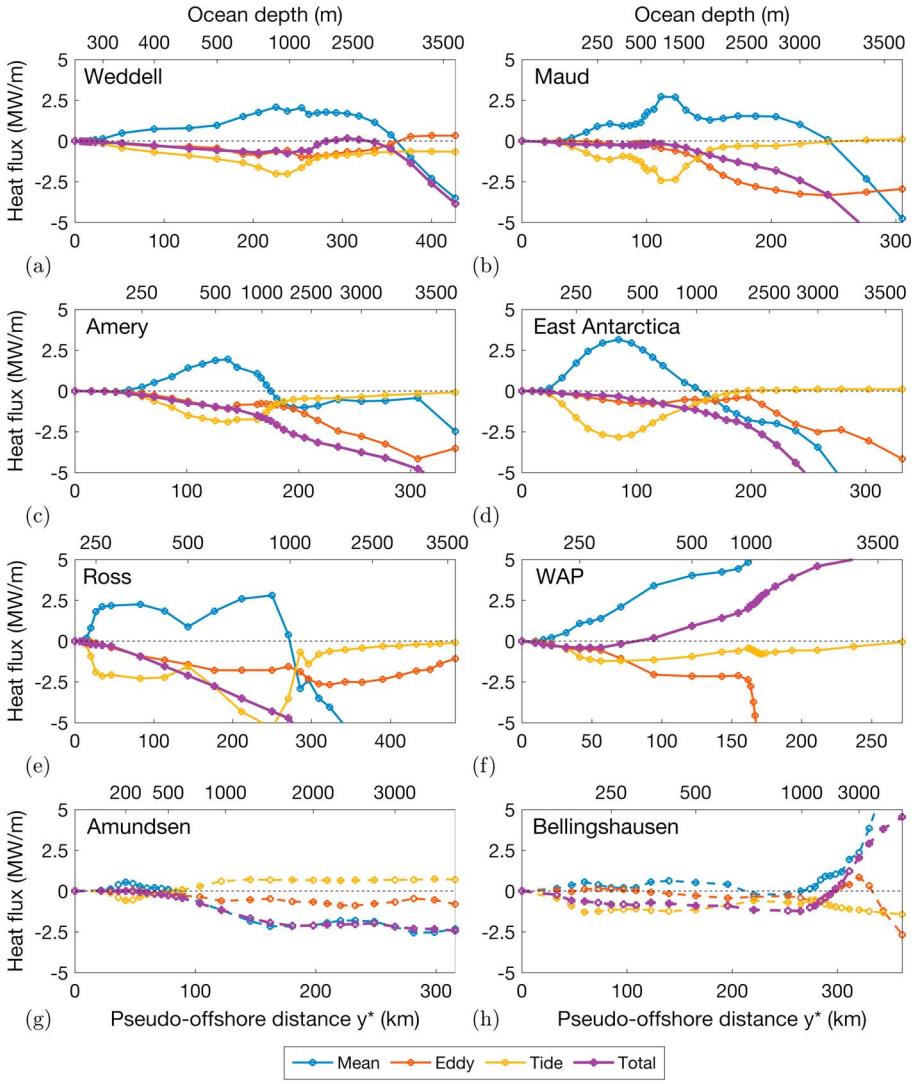

Figure 2. (a–h) Depth-integrated offshore heat flux in each of the Antarctic sectors illustrated in Figure 1. In each panel the heat flux is decomposed into components due to mean flows, eddies, and tides, as described in the text. In each panel the ordinate is given both in bathymetric coordinates (upper axis) and in a pseudo-offshore coordinate system that approximates true distance from the Antarctic coast (lower axis). In Figures 2g and 2h we indicate heat flux magnitudes using dashed lines because the lack of high-resolution bathymetric data in these sectors (Smith & Sandwell, 1997) has likely distorted the results.

requires the use of hundreds of compute cores for several days, even after the process has been optimized for computational efficiency. However, our decomposition (1) is supported by qualitative and quantitative differences between the diagnosed eddy and "tidal" components of the flow, for example, in their relative kinetic energies (Figures 3d and 3e). Furthermore, spectral analysis of the potential temperature, salinity, and kinetic energy demonstrates that daily averaging effectively removes high-frequency variability associated with the tides (see supporting information Figure S2). Also, for reasons of computational efficiency, the heat flux terms in (2) were computed using 6-hourly snapshots of the model state. We selected this frequency based on a convergence study that shows that using higher-frequency output data yields essentially no difference in the eddy/tidal kinetic energy and cross-isobath heat flux (see supporting information Figure S3).

3. Shoreward Heat Transport Across the Antarctic Slope Front

We first quantify shoreward heat transport by mean flows, eddies, and tides around the entire Antarctic continent. There is pronounced spatial heterogeneity in the shelf water masses (Whitworth et al., 1998), so we

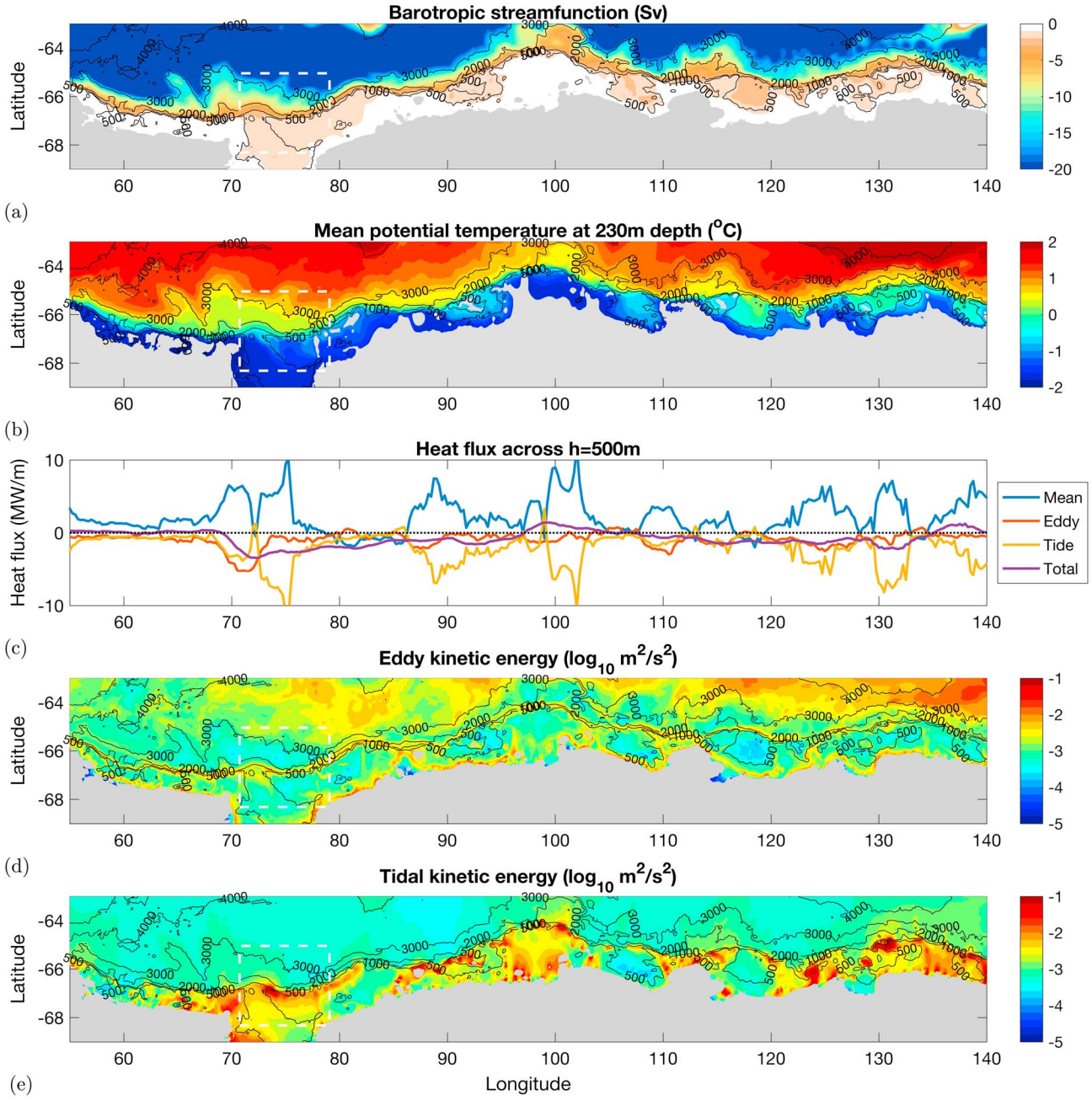

Figure 3. Along-coast localization of heat fluxes in the combined Amery/East Antarctica sectors. (a) Barotropic stream function. (b) Time-mean potential temperature at 230 m depth. (c) Offshore heat fluxes as a function of longitude, decomposed into mean, eddy, and tidal components (see text for details). (d, e) Eddy kinetic energy and tidal kinetic energy, respectively. In Figures 3a, 3b, 3d, and 3e the black contours indicate the ocean depth in meters and the white dashed box indicates the test region used to verify our analysis techniques in supporting information Figures S2 and S3.

divide the Antarctic margins into eight regions, shown in Figure 1. The results are not qualitatively sensitive to changes in the boundaries of these sectors, as evidenced by the similarity in the cross-slope heat fluxes shown in Figure 2. For the sake of completeness, Figure 2 includes results from the Amundsen and Bellingshausen sectors. Herein, however, we do not discuss these results further because the model's bathymetric product (Smith & Sandwell, 1997) lacks measurements in these sectors (see supporting information Figure S1), leading to computed heat fluxes that are expected to diverge qualitatively from those occurring in the real ocean.

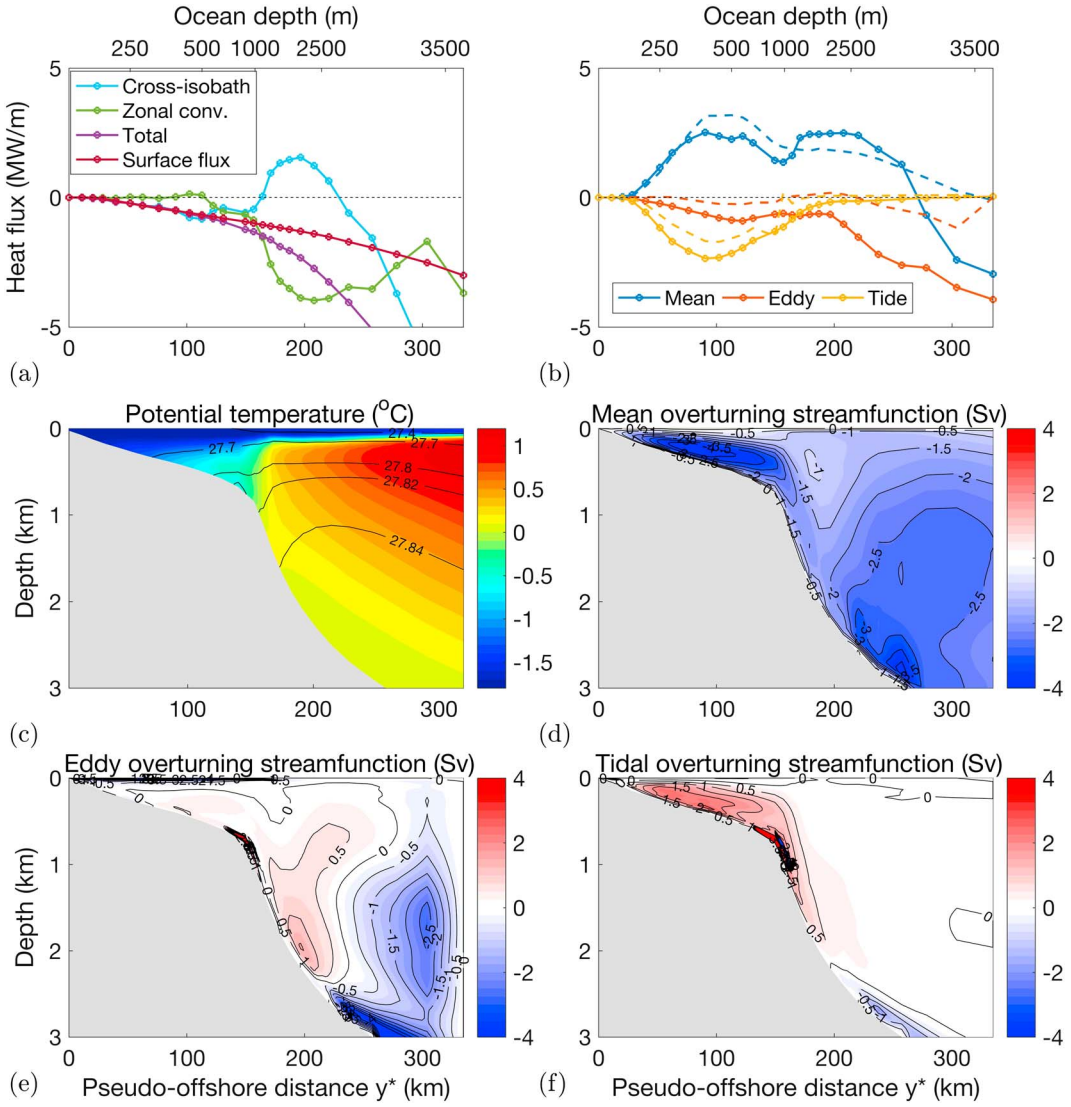

Figure 4. (a, b) Offshore heat fluxes in the combined Amery/East Antarctica sections (see Figure 1). (c) Time- and longshore-averaged potential temperature (colors) and potential density (black contours). (d–f) Approximations to the mean, eddy, and tidal components of the overturning streamfunction, respectively. In Figure 4a we decompose the total heat flux (purple) into components due to true cross-isobath heat fluxes (light blue) and due to zonal advective convergence (green). The total heat flux is also compared to the surface heat flux integrated from the coast (dark red); mismatch between the total heat flux and surface heat flux curves indicates a time tendency in the ocean heat content. In Figure 4b we decompose the cross-isobath component of the heat flux into mean, eddy, and tidal components. The dashed lines show estimates of the heat fluxes, constructed by combining the time- and longshore-averaged temperature with the overturning streamfunctions shown in Figures 4d–4f.

Calculation of shoreward heat flux is hindered by the convoluted shape of the Antarctic continental slope and coastline, so we transform the model output data to a coordinate system that follows isobaths in each sector of the Antarctic margins. For example, for the total advective heat flux $\boldsymbol{F}_\theta$ we define the total offshore flux as

$$f_\theta(h_0) = \langle \boldsymbol{F}_\theta \rangle_{h_0} = \frac{1}{L} \iint_{h<h_0} \nabla \cdot \boldsymbol{F}_\theta \, \mathrm{d}A \,, \tag{3}$$

where h is the ocean depth, $z = -h_0$ is a selected isobath, and dA denotes an infinitesimal area. For presentation purposes we convert the total offshore heat flux to a heat flux per unit along-shelf distance

by dividing by a length L that approximately measures the length of the continental shelf break in each sector (see supporting information Table S1). We also present the heat fluxes as functions of a quasi-offshore coordinate $y^\star$ via

$$y^\star(h_0) = \frac{1}{L}\iint_{h<h_0} 1\,\mathrm{d}A\,. \tag{4}$$

The resulting heat fluxes and their cross-slope profiles are quantitatively sensitive to the method of estimating L, so we avoid direct comparisons between offshore heat fluxes per unit length in different sectors. Note that f_θ includes both heat fluxes across the isobath $z = -h_0$ and heat flux convergence across the boundaries of the sector, the latter being almost entirely due to along-shelf/slope mean circulation rather than eddies or tides. In supporting information Figure S4 we decompose the total heat flux into components due to cross-isobath fluxes and along-shelf/slope convergence. Note also that the seafloor depth does not always vary monotonically from the coast to the deep ocean; local maxima/minima of seafloor depth may make a contribution to the heat flux computed using (3). We have partly ameliorated this issue by choosing the sectors shown in Figure 1 to avoid shallower areas and seamounts offshore of the continental slope, like Maud Rise and Kerguelen Plateau, but the cross-isobath heat flux close to the coast on the continental shelf may include contributions associated with small islands and seamounts.

Figure 2 shows the depth-integrated cross-isobath heat fluxes in all eight sectors of the Antarctic continental shelf and slope, decomposed into mean, eddy, and tidal components. The heat flux profiles are qualitatively consistent between sectors that have a strong ASF (Weddell, Maud, Amery, East Antarctica, and Ross). Shoreward heat flux is typically dominated by eddies over the continental slope ($h \gtrsim 1{,}500$ m) and by tides across the continental shelf break 500 m $\lesssim h \lesssim$ 1,000 m. However, the tidal shoreward heat flux is largely compensated by a mean offshore heat flux; in the Maud, Amery, East Antarctica, and Weddell sectors, the mean and tidal heat fluxes across the 500 m isobath differ by less than 10%, 3%, 9%, and 13%, respectively. This results in close agreement between the shoreward eddy heat flux and the net heat flux in all of these sectors. On the continental slope the mean heat flux becomes negative due to zonal convergence (see supporting information Figure S4); that is, warmer water is carried in through each sector's eastern boundary than is carried out through the western boundary. Over the West Antarctic Peninsula (WAP) the tidal heat flux is relatively weak due to low tidal amplitudes in this sector (e.g., Lyard et al., 2006), so the dominant balance is between shoreward eddy heat flux and offshore mean heat flux. In this sector the total heat flux f_θ is positive due to alongshore heat flux divergence (see supporting information Figure S4); southward flow carries colder water into the WAP sector at its northern edge and warmer water out at its southern edge.

4. Localization of Heat Transport Across the Shelf Break

We now examine how shoreward heat fluxes are locally distributed, both as a function of depth and a function of along-slope distance. Due to the qualitative similarity between the processes governing cross-isobath heat transport in different sectors of Antarctic margins (Figure 2), we focus on the combined Amery/East Antarctica sectors, where the near-zonal coastline facilitates interpretation of heat flux localization. Additionally, intrusion of CDW and relatively high basal melt rates has been diagnosed beneath some of the ice shelves in this region (Rintoul et al., 2016; Silvano et al., 2017). Figures 3a and 3b illustrate this sector via the time-averaged model barotropic streamfunction and potential temperature at 230 m depth. The circulation is dominated by the westward ASC, which closely follows isobaths, leading to shoreward excursion in coastal troughs. The ASC is associated with an $\mathcal{O}(3°\mathrm{C})$ change in potential temperature across the 100–200 km wide continental slope, within which the ASF is characterized by a temperature change of approximately $\mathcal{O}(2°\mathrm{C})$ over less than 50 km (e.g., Meijers et al., 2010). Figures 4a and 4b show contributions to the heat budget in this sector.

We first derive an approximate measure of cross-isobath heat flux localization by extending the method described in section 3. Figure 3c shows the heat flux f_θ across $h = 500$ m, which typically lies close to the shelf break and the isobath across which shoreward tidal heat fluxes are maximal, computed in running zonal windows that are 3° wide in longitude and plotted every 0.25°. This serves to smooth out small-scale zonal variations in the heat fluxes and so likely underestimates their most extreme fluctuations. In these relatively short zonal windows there is substantial compensation between the offshore/shoreward cross-isobath mean heat flux and zonal heat flux convergence/divergence, which individually exhibit larger fluctuations than those shown in Figure 3c (not shown). In contrast, the eddy and tidal components of this localized heat flux accurately quantify flux across isobaths. Local heat fluxes across other isobaths exhibit qualitatively similar zonal localization.

Figure 3c shows that the mean/tidal heat flux compensation found in each sector of the Antarctic margins (Figure 2) also holds as a function of along-slope distance (Pearson's correlation coefficient $r = -0.86$). In contrast, though the integrated eddy and total heat fluxes match closely, locally, they are weakly related ($r = 0.31$). A tempting interpretation is that tides draw heat out of the slope current and transfer it shoreward, leading to a series of decreases in the temperature of the current as it flows westward along isobaths. However, Figure 4a shows that the net along-isobath heat flux convergence on this isobath is negligible; below we show that the tidal heat fluxes are in fact countered by a mean overturning circulation. In Figures 3c–3e the cross-isobath heat fluxes are compared against the eddy and tidal components of the kinetic energy (EKE and TKE, respectively), computed analogously to (1). The EKE is elevated in a narrow strip along the core of the ASF and north of the continental slope in the ACC but is not substantially localized as a function of along-slope distance. In contrast, TKE is elevated along the shelf break, particularly in the vicinity of a number of bathymetric features (note the logarithmic color bar in Figure 3e). These regions of elevated TKE coincide with the "hot spots" of shoreward tidal heat transport shown in Figure 3c.

We now examine how the shoreward heat flux is distributed in the vertical and in particular the roles of mean, eddy, and tidal overturning circulations in transferring heat across isobaths. We first define an along-isobath averaging operator for scalar quantities, for example, potential temperature:

$$\langle \theta \rangle_{h_0} = \frac{1}{L} \frac{\mathrm{d}}{\mathrm{d}y^\star} \iint_{h<h_0} \theta \, \mathrm{d}A. \tag{5}$$

Here we have used the same notation for the averaging operator $\langle \bullet \rangle_{h_0}$ as in (3) to simplify the presentation, with the understanding that this operation follows (3) for vector quantities and (5) for scalar quantities. We then construct approximate mean, eddy, and tidal overturning stream functions using the Transformed Eulerian Mean (TEM) formalism (Plumb & Ferrari, 2005; Wolfe, 2014)

$$\psi(h_0) = \underbrace{\int_z^0 \left\langle \overline{\boldsymbol{u}}^{t,e} \right\rangle_{h_0} \mathrm{d}z'}_{\psi_{\mathrm{mean}}} + \underbrace{\frac{\left\langle \overline{\boldsymbol{u}_e b_e}^{e} \right\rangle_{h_0}}{\partial_z \left\langle \overline{b}^{t,e} \right\rangle_{h_0}}}_{\psi_{\mathrm{eddy}}} + \underbrace{\frac{\left\langle \overline{\boldsymbol{u}_t b_t}^{t,e} \right\rangle_{h_0}}{\partial_z \left\langle \overline{b}^{t,e} \right\rangle_{h_0}}}_{\psi_{\mathrm{tide}}}, \tag{6}$$

where b is the buoyancy and ∂_z denotes a vertical derivative. Equation (6) differs from the usual TEM only in that the transient lateral buoyancy flux has been decomposed exactly into eddy and tidal components following (2). In practice, we compute buoyancy fluctuations and mean buoyancy gradient using locally referenced potential density (McIntosh & McDougall, 1996; Stewart & Thompson, 2015a).

Figure 4c shows the along-isobath mean potential temperature $\left\langle \overline{\theta}^{t,e} \right\rangle_{h_0}$ and surface-referenced potential density. Our averaging operator (5) captures the structure of the ASF, though the front is somewhat smoother than in individual transects (see, e.g., Meijers et al., 2010) because the flow deviates slightly across isobaths as it traverses this sector. Figures 4d–4f show the mean, eddy, and tidal overturning stream functions computed via (6), with red colors corresponding to clockwise flow along streamlines and blue colors corresponding to counterclockwise flow. Consistent with Figure 4b, the eddy-driven and tidally-driven circulations transfer deeper, warmer water toward the coast and shallower, colder water offshore, leading to a net shoreward heat flux. The mean overturning circulation directly opposes the eddy and tidal overturning circulations and therefore transfers heat offshore. Note that further offshore, the mean streamfunction includes a component associated with changes in the vertical structure of the along-isobath volume transports passing through the zonal boundaries of this sector (see Figure 4a).

The strength of the mean circulation across the shelf break greatly exceeds the shoreward Ekman transport due to the easterly winds (see, e.g., Spence et al., 2014; Stewart & Thompson, 2012). The strength of the Ekman overturning circulation can be estimated as $\psi_{\mathrm{Ekman}} = -\left\langle \overline{\tau_x}^{t,e} \right\rangle_{h_0} / (\rho_0 f)$, where τ_x is the zonal wind stress, f is the Coriolis parameter, and ρ_0 is a reference density for the ocean (Marshall & Radko, 2003). Combining $\left\langle \overline{\tau_x}^{t,e} \right\rangle_{h_0} \approx -0.07\ \mathrm{N\ m^{-2}}$ at the shelf break with $f \approx -1.3 \times 10^{-4}\ \mathrm{rad\ s^{-1}}$ and $\rho_0 = 1027\ \mathrm{kg\ m^{-3}}$, we estimate that the wind-driven mean overturning circulation in the Amery/East Antarctica sectors is 2.2 Sverdrups (Sv), less than half of the diagnosed mean overturning circulation of 4.6 Sv across the shelf break. Geostrophic mean flows are unlikely to contribute to the mean overturning circulation because they are strongly constrained to follow isobaths (see Figure 3a); the net cross-isobath volume flux is only 0.1 Sv in this sector. This suggests that the cross-isobath mean overturning over the shelf and slope is primarily due to eddy/tidal momentum flux

convergence. However, we are unable to distinguish the drivers of the mean overturning circulation based on the evidence presented here. A quantitative evaluation of these drivers will likely require a separate analysis of the vorticity budget, as the momentum budget is complicated by the large variations in bathymetry and mean flow orientation.

The dashed lines in Figure 4b indicate estimated cross-isobath heat fluxes calculated by combining the stream functions defined in (6) with the along-isobath mean potential temperature $\left\langle \overline{\theta}^{t,e} \right\rangle_{h_0}$ shown in Figure 4c, for example,

$$f_\psi(h_0) = \int_{-h_0}^{0} -\left\langle \overline{\theta}^{t,e} \right\rangle_{h_0} \frac{\partial \psi}{\partial z} \, \mathrm{d}z. \tag{7}$$

This approach makes use of approximate overturning stream functions (6) and does not take into account along-shore variations in the components of the cross-isobath transport nor the thermohaline structure of the front. Despite this, the estimated cross-isobath mean and tidal heat fluxes are within ~25% of the heat fluxes diagnosed directly via (3). In contrast, the eddy heat fluxes estimates from the overturning circulation are approximately zero and do not explain the shoreward eddy heat transport. This suggests that the cross-isobath eddy heat flux is due to eddy stirring of heat along density surfaces (e.g., Stewart & Thompson, 2016) or along the ocean bed (Nøst et al., 2011) rather than the ageostrophic eddy-driven overturning circulation. Similar results are found in the Maud, Weddell, Ross, and even WAP sectors.

5. Discussion

In this study we have used the first ocean/sea ice model capable of resolving circum-Antarctic mean flows, eddies, and tides to quantify the relative contributions of these processes to shoreward heat transport. We have emphasized the sectors of the Antarctic margins that host a strong ASF (around 75% of the continental slope), in which eddies support heat transfer across the continental slope but are surpassed by tidal fluxes across the shelf break (Figure 2). The tidal heat transfer is confined to "hot spots" in the vicinity of a few bathymetric features along the shelf break but is locally compensated by offshore mean heat fluxes (Figure 3). This results in a close agreement between the shoreward eddy heat flux and the total shoreward heat flux (Figure 2). We linked the opposing mean/tidal heat fluxes to compensating mean and tidally driven overturning circulations across the shelf break (Figure 4) but found that the eddy-driven overturning circulation could not explain the shoreward eddy flux. Taken together, these results indicate that eddy stirring along isopycnals or along the ocean bed is the mechanism that transfers heat across most of the ASF (Nøst et al., 2011; Stewart & Thompson, 2016) but that the ASF's structure and overturning circulation are strongly modulated by tides (Flexas et al., 2015). However, there remains some uncertainty as to the exact mechanism of eddy heat transport due to our approximate construction of the overturning circulation in equation (6).

While the LLC_4320 and LLC_2160 simulations offer a unique circum-Antarctic insight into the role of high-frequency processes in facilitating shoreward heat flux, they carry several caveats. We have not discussed cross-isobath heat fluxes diagnosed from the Bellingshausen and Amundsen Seas because the model's bathymetric product lacks high-resolution measurements in those sectors (Smith & Sandwell, 1997). Specifically, the continental shelf and slope are smooth, lacking features such as troughs that have been shown to be critical in guiding CDW onto the continental shelf (e.g., St-Laurent et al., 2013; Thoma et al., 2008). While troughs efficiently steer the slope current shoreward, the relatively small cross-isobath heat fluxes diagnosed within the troughs suggest that they do not efficiently draw heat across isobaths (Figures 3a and 3b). However, some of the troughs extend far into the ice shelf cavities (e.g., Hattermann et al., 2014; Nicholls et al., 2009), in which cases inflowing CDW need not ascend to depths much shallower than the shelf break in order to reach the bases of the ice shelves. The LLC_4320 and LLC_2160 simulations cannot reproduce this mechanism because they do not include ice shelf cavities. However, waters reaching these troughs must still cross the continental slope and shelf break, and so their route from the open ocean can still be captured using our bathymetric coordinate transformation (3).

Another key caveat of the LLC_4320 and LLC_2160 simulations is their short durations of 1 and 2 years, respectively. As discussed in section 2, the quantitative similarity between results derived from these simulations suggests that their durations are sufficiently long to derive converged eddy/tidal statistics. However, the model state is drifting, as evidenced by the mismatch between the diagnosed net shoreward heat fluxes and the integrated surface heat fluxes toward the bottom of the continental slope in Figure 4a

and supporting information Figure S4. Quantitative changes in the heat fluxes should therefore be expected if the model integration were continued for longer, potentially adjusting over thousands of years as the global overturning circulation adjusted to the surface boundary conditions (Hirst et al., 2000). However, it is not clear that such an equilibrated state would provide a more realistic representation of the stratification and thus the eddy/tidal heat fluxes. The model's short duration also implies that it undersamples the interannual variability in the atmospheric circulation, which responds to global modes of atmospheric variability like the El Niño–Southern Oscillation and the Southern Annular Mode (Langlais et al., 2015) and to which the ASF has been shown to be sensitive (Nøst et al., 2011; Stewart & Thompson, 2013). Longer simulations will be required to adequately sample these modes of variability and also to allow eddy variability to be separated from seasonal variability, which also projects onto cross-slope water mass exchanges and heat transport (Su et al., 2014; Wang et al., 2012; Zhou et al., 2014).

Though longer simulations at similar resolution would permit a greatly expanded range of science questions to be addressed, the consistency of our key findings between sectors of the Antarctic margins suggests that the relative roles of mean flows, eddies, and tides are unlikely to change. These finding raise further questions regarding the dynamical roles of eddies and tides in shaping the ASF and cross-slope exchanges. For example, approximate compensation between the mean and tidal overturning stream functions (see Figure 4) might be expected to result from a tidal "Stokes drift" opposed by a tidally driven rectified mean flow, leading to a relatively small cross-isobath tidal residual flow (Robinson, 1981, 1983). However, our scaling analysis in section 4 suggests that almost 50% of the mean overturning circulation may be due attributed to wind-driven Ekman transport. It is therefore unclear why there should be such a close compensation between the mean and tidal cross-isobath heat fluxes (Figures 2–4). Similarly, while our results collectively suggest that eddy stirring of potential temperature dominates the overall shoreward heat flux, the two simulations analyzed here offer limited insight into the sensitivity of this heat flux to ongoing changes in stratification (e.g., Schmidtko et al., 2014) or atmospheric conditions (e.g., Spence et al., 2014). Additional process-oriented modeling of the ASF will likely be required to achieve a complete characterization of these phenomena.

Acknowledgments
This material is based in part upon work supported by the National Science Foundation under grants OCE-1538702 and PLR-1543388. A. K. was supported by the Australian Research Council Discovery Early Career Researcher Award (DE140100076). D. M. carried out this work at the Jet Propulsion Laboratory (JPL), California Institute of Technology, under a contract with the National Aeronautics and Space Administration (NASA). High-end computing resources were provided by the NASA Advanced Supercomputing (NAS) Division of the Ames Research Center. The authors thank the MITgcm development team, NAS computer scientists, and SGI engineers for their contributions in producing and making available the high-resolution model output used in this study. The model configuration files can be downloaded from http://wwwcvs.mitgcm.org/viewvc/MITgcm/MITgcm_contrib/llc_hires/llc_4320/. The raw model output data are stored on NASA's Pleiades supercomputer and may be accessed via request to D. M. The time-averaged model output fields used to derive the results presented in this manuscript can be downloaded from https://doi.org/10.4226/77/5a37035ea15b2. The authors thank three anonymous reviewers for comments that improved the manuscript.

References

Ardhuin, F., Gille, S. T., Menemenlis, D., Rocha, C. B., Rascle, N., Chapron, B., … Molemaker, J. (2017). Small-scale open ocean currents have large effects on wind wave heights. *Journal of Geophysical Research: Oceans*, *122*, 4500–4517. https://doi.org/10.1002/2016JC012413

Arthern, R. J., Winebrenner, D. P., & Vaughan, D. G. (2006). Antarctic snow accumulation mapped using polarization of 4.3-cm wavelength microwave emission. *Journal of Geophysical Research*, *111*, D06107. https://doi.org/10.1029/2004JD005667

Arzeno, I. B., Beardsley, R. C., Limeburner, R., Owens, B., Padman, L., Springer, S. R., … Williams, M. J. M. (2014). Ocean variability contributing to basal melt rate near the ice front of Ross Ice Shelf, Antarctica. *Journal of Geophysical Research: Oceans*, *119*, 4214–4233. https://doi.org/10.1002/2014JC009792

Couto, N., Martinson, D. G., Kohut, J., & Schofield, O. (2017). Distribution of Upper Circumpolar Deep Water on the warming continental shelf of the West Antarctic Peninsula. *Journal of Geophysical Research: Oceans*, *122*, 5306–5315. https://doi.org/10.1002/2017JC012840

Daru, V., & Tenaud, C. (2004). High order one-step monotonicity-preserving schemes for unsteady compressible flow calculations. *Journal of Computational Physics*, *193*(2), 563–594.

DeConto, R. M., & Pollard, D. (2016). Contribution of Antarctica to past and future sea-level rise. *Nature*, *531*(7596), 591–597.

Dinniman, M. S., Asay-Davis, X. S., Galton-Fenzi, B. K., Holland, P. R., Jenkins, A., & Timmermann, R. (2016). Modeling ice shelf/ocean interaction in Antarctica: A review. *Oceanography*, *29*(4), 144–153.

Dufour, C. O., Griffies, S. M., de Souza, G. F., Frenger, I., Morrison, A. K., Palter, J. B., … Anderson, W. G. (2015). Role of mesoscale eddies in cross-frontal transport of heat and biogeochemical tracers in the Southern Ocean. *Journal of Physical Oceanography*, *45*(12), 3057–3081.

European Centre for Medium-Range Weather Forecasts (2011). ECMWF's Operational Model Analysis starting in 2011.

Fekete, B. M., Vörösmarty, C. J., & Grabs, W. (2002). High-resolution fields of global runoff combining observed river discharge and simulated water balances. *Global Biogeochemical Cycles*, *16*(3), 1042.

Ferrari, R., Jansen, M. F., Adkins, J. F., Burke, A., Stewart, A. L., & Thompson, A. F. (2014). Antarctic sea ice control on ocean circulation in present and glacial climates. *Proceedings of the National Academy of Sciences of the United States of America*, *111*(24), 8753–8758.

Flexas, M., Schodlok, M. P., Padman, L., Menemenlis, D., & Orsi, A. H. (2015). Role of tides on the formation of the Antarctic Slope Front at the Weddell-Scotia Confluence. *Journal of Geophysical Research: Oceans*, *120*, 3658–3680. https://doi.org/10.1002/2014JC010372

Flierl, G. R., & McWilliams, J. C. (1977). On the sampling requirements for measuring moments of eddy variability. *Journal of Marine Research*, *35*, 797–820.

Foldvik, A., Middleton, J. H., & Foster, T. D. (1990). The tides of the southern Weddell Sea. *Deep Sea Research Part A. Oceanographic Research Papers*, *37*(8), 1345–1362.

Foreman, M. G. G., & Henry, R. F. (1989). The harmonic analysis of tidal model time series. *Advances in Water Resources*, *12*(3), 109–120.

Forget, G., Campin, J.-M., Heimbach, P., Hill, C. N., Ponte, R. M., & Wunsch, C. (2015). ECCO version 4: An integrated framework for non-linear inverse modeling and global ocean state estimation. *Geoscientific Model Development*, *8*, 3071–3104.

Fox-Kemper, B., & Menemenlis, D. (2008). Can large eddy simulation techniques improve mesoscale rich ocean models? *Geophysical Monograph Series*, *177*, 319–338.

Gordon, A. L., Orsi, A. H., Muench, R., Huber, B. A., Zambianchi, E., & Visbeck, M. (2009). Western ross sea continental slope gravity currents. *Deep-Sea Research Part II: Topical Studies in Oceanography*, *56*(13), 796–817.

Gordon, A. L., Zambianchi, E., Orsi, A., Visbeck, M., Giulivi, C. F., Whitworth, T., & Spezie, G. (2004). Energetic plumes over the western Ross Sea continental slope. *Geophysical Research Letters*, *31*, L21302. https://doi.org/10.1029/2004GL020785

Graham, J. A., Dinniman, M. S., & Klinck, J. M. (2016). Impact of model resolution for on-shelf heat transport along the West Antarctic Peninsula. *Journal of Geophysical Research: Oceans*, *121*, 7880–7897. https://doi.org/10.1002/2016JC011875

Graham, J. A., Heywood, K. J., Chavanne, C. P., & Holland, P. R. (2013). Seasonal variability of water masses and transport on the Antarctic continental shelf and slope in the southeastern Weddell Sea. *Journal of Geophysical Research: Oceans*, *118*, 2201–2214. https://doi.org/10.1002/jgrc.20174

Hallberg, R. (2013). Using a resolution function to regulate parameterizations of oceanic mesoscale eddy effects. *Ocean Modelling*, *72*, 92–103.

Hattermann, T., Smedsrud, L. H., Nøst, O. A., Lilly, J. M., & Galton-Fenzi, B. K. (2014). Eddy-resolving simulations of the Fimbul Ice Shelf cavity circulation: Basal melting and exchange with open ocean. *Ocean Modelling*, *82*, 28–44.

Hellmer, H. H., Kauker, F., Timmermann, R., Determann, J., & Rae, J. (2012). Twenty-first-century warming of a large Antarctic ice-shelf cavity by a redirected coastal current. *Nature*, *485*(7397), 225–228.

Hellmer, H. H., Kauker, F., Timmermann, R., & Hattermann, T. (2017). The fate of the southern Weddell Sea continental shelf in a warming climate. *Journal of Climate*, *30*(12), 4337–4350.

Heywood, K. J., Biddle, L. C., Boehme, L., Dutrieux, P., Fedak, M., Jenkins, A., … Naveira Garabato, A. C. (2016). Between the devil and the deep blue sea: The role of the Amundsen Sea continental shelf in exchanges between ocean and ice shelves. *Oceanography*, *29*(4), 118–129.

Hirst, A. C., O'Farrell, S. P., & Gordon, H. B. (2000). Comparison of a coupled ocean-atmosphere model with and without oceanic eddy-induced advection. Part I: Ocean spinup and control integrations. *Journal of Climate*, *13*(1), 139–163.

Jackett, D. R., & Mcdougall, T. J. (1995). Minimal adjustment of hydrographic profiles to achieve static stability. *Journal of Atmospheric and Oceanic Technology*, *12*(2), 381–389.

Jacobs, S. S. (1991). On the nature and significance of the Antarctic Slope Front. *Marine Chemistry*, *35*(1), 9–24.

Jenkins, A., Dutrieux, P., Jacobs, S., Steig, E. J., Gudmundsson, G. H., Smith, J., & Heywood, K. J. (2016). Decadal ocean forcing and Antarctic ice sheet response: Lessons from the Amundsen Sea. *Oceanography*, *29*(4), 106–117.

Jourdain, N. C., Mathiot, P., Merino, N., Durand, G., Le Sommer, J., Spence, P., … Madec, G. (2017). Ocean circulation and sea-ice thinning induced by melting ice shelves in the Amundsen Sea. *Journal of Geophysical Research: Oceans*, *122*, 2550–2573. https://doi.org/10.1002/2016JC012509

Langlais, C. E., Rintoul, S. R., & Zika, J. D. (2015). Sensitivity of Antarctic Circumpolar Current transport and eddy activity to wind patterns in the Southern Ocean. *Journal of Physical Oceanography*, *45*(4), 1051–1067.

Lyard, F., Lefevre, F., Letellier, T., & Francis, O. (2006). Modelling the global ocean tides: Modern insights from FES2004. *Ocean Dynamics*, *56*(5-6), 394–415.

MacAyeal, D. R. (1984). Thermohaline circulation below the Ross Ice Shelf: A consequence of tidally induced vertical mixing and basal melting. *Journal of Geophysical Research*, *89*(C1), 597–606.

Mack, S. L., Dinniman, M. S., McGillicuddy, D. J., Sedwick, P. N., & Klinck, J. M. (2017). Dissolved iron transport pathways in the Ross Sea: Influence of tides and horizontal resolution in a regional ocean model. *Journal of Marine Systems*, *166*, 73–86.

Marshall, J., Adcroft, A., Hill, C., Perelman, L., & Heisey, C. (1997). A finite-volume, incompressible Navier Stokes model for studies of the ocean on parallel computers. *Journal of Geophysical Research*, *102*, 5753–5766.

Marshall, J., Hill, C., Perelman, L., & Adcroft, A. (1997). Hydrostatic, quasi-hydrostatic, and nonhydrostatic ocean modeling. *Journal of Geophysical Research*, *102*, 5733–5752.

Marshall, J., & Radko, T. (2003). Residual-mean solutions for the Antarctic Circumpolar Current and its associated overturning circulation. *Journal of Physical Oceanography*, *33*(11), 2341–2354.

Martinson, D. G., & McKee, D. C. (2012). Transport of warm Upper Circumpolar Deep Water onto the western Antarctic Peninsula continental shelf. *Ocean Science*, *8*(4), 433–442.

McIntosh, P. C., & McDougall, T. J. (1996). Isopycnal averaging and the residual mean circulation. *Journal of Physical Oceanography*, *26*(8), 1655–1660.

Meijers, A. J. S., Klocker, A., Bindoff, N. L., Williams, G. D., & Marsland, S. J. (2010). The circulation and water masses of the Antarctic shelf and continental slope between 30 and 80°E. *Deep-Sea Research Part II*, *57*(9), 723–737.

Millan, R., Rignot, E., Bernier, V., Morlighem, M., & Dutrieux, P. (2017). Bathymetry of the Amundsen Sea Embayment sector of West Antarctica from Operation IceBridge gravity and other data. *Geophysical Research Letters*, *44*, 1360–1368. https://doi.org/10.1002/2016GL072071

Nakayama, Y., Timmermann, R., Rodehacke, C. B., Schröder, M., & Hellmer, H. H. (2014). Modeling the spreading of glacial meltwater from the Amundsen and Bellingshausen Seas. *Geophysical Research Letters*, *41*, 7942–7949. https://doi.org/10.1002/2014GL061600

Naveira Garabato, A. C., Zika, J. D., Jullion, L., Brown, P. J., Holland, P. R., Meredith, M. P., & Bacon, S. (2016). The thermodynamic balance of the Weddell Gyre. *Geophysical Research Letters*, *43*, 317–325. https://doi.org/10.1002/2015GL066658

Nicholls, K. W., Østerhus, S., Makinson, K., Gammelsrød, T., & Fahrbach, E. (2009). Ice-ocean processes over the continental shelf of the southern Weddell Sea, Antarctica: A review. *Reviews of Geophysics*, *47*, RG3003. https://doi.org/10.1029/2007RG000250

Nøst, O. A., Biuw, M., Tverberg, V., Lydersen, C., Hattermann, T., Zhou, Q., … Kovacs, K. M. (2011). Eddy overturning of the Antarctic Slope Front controls glacial melting in the Eastern Weddell Sea. *Journal of Geophysical Research*, *116*, C11014. https://doi.org/10.1029/2011JC006965

Orsi, A. H., Jacobs, S. S., Gordon, A. L., & Visbeck, M. (2001). Cooling and ventilating the Abyssal Ocean. *Geophysical Research Letters*, *28*(15), 2923–2926.

Orsi, A. H., Whitworth, T., & Nowlin, W. D. (1995). On the meridional extent and fronts of the Antarctic Circumpolar Current. *Deep Sea Research Part I: Oceanographic Research Papers*, *42*(5), 641–673.

Padman, L., Howard, S. L., Orsi, A. H., & Muench, R. D. (2009). Tides of the northwestern Ross Sea and their impact on dense outflows of Antarctic Bottom Water. *Deep Sea Research Part II: Topical Studies in Oceanography*, *56*(13), 818–834.

Plumb, R. A., & Ferrari, R. (2005). Transformed Eulerian-mean theory. Part I: Nonquasigeostrophic theory for eddies on a zonal-mean flow. *Journal of Physical Oceanography*, *35*(2), 165–174.

Purkey, S. G., & Johnson, G. C. (2013). Antarctic Bottom Water warming and freshening: Contributions to sea level rise, ocean freshwater budgets, and global heat gain. *Journal of Climate*, *26*(16), 6105–6122.

Rignot, E., & Jacobs, S. S. (2002). Rapid bottom melting widespread near Antarctic ice sheet grounding lines. *Science*, *296*(5575), 2020–2023.

Rintoul, S. R., Silvano, A., Pena-Molino, B., van Wijk, E., Rosenberg, M., Greenbaum, J. S., & Blankenship, D. D. (2016). Ocean heat drives rapid basal melt of the Totten Ice Shelf. *Science Advances*, *2*(12), E1601610.

Robertson, R. (2001). Internal tides and baroclinicity in the southern Weddell Sea: 1. Model description. *Journal of Geophysical Research*, *106*(C11), 27,001–27,016. https://doi.org/10.1029/2000JC000475

Robinson, I. S. (1981). Tidal vorticity and residual circulation. *Deep Sea Research Part A. Oceanographic Research Papers*, *28*(3), 195–212.
Robinson, I. S. (1983). Tidally induced residual flows. *Elsevier Oceanography Series*, *35*, 321–356.
Rocha, C. B., Chereskin, T. K., Gille, S. T., & Menemenlis, D. (2016). Mesoscale to submesoscale wavenumber spectra in Drake Passage. *Journal of Physical Oceanography*, *46*(2), 601–620.
Schmidtko, S., Heywood, K. J., Thompson, A. F., & Aoki, S. (2014). Multidecadal warming of Antarctic waters. *Science*, *346*(6214), 1227–1231.
Schodlok, M. P., Menemenlis, D., & Rignot, E. J. (2016). Ice shelf basal melt rates around Antarctica from simulations and observations. *Journal of Geophysical Research: Oceans*, *121*, 1085–1109. https://doi.org/10.1002/2015JC011117
Silvano, A., Rintoul, S. R., Peña-Molino, B., & Williams, G. D. (2017). Distribution of water masses and meltwater on the continental shelf near the Totten and Moscow University ice shelves. *Journal of Geophysical Research: Oceans*, *122*, 2050–2068. https://doi.org/10.1002/2016JC012115
Smith, K. S., & Vallis, G. K. (2001). The scales and equilibration of midocean eddies: Freely evolving flow. *Journal of Physical Oceanography*, *31*(2), 554–571.
Smith, W. H. F., & Sandwell, D. T. (1997). Global sea floor topography from satellite altimetry and ship depth soundings. *Science*, *277*(5334), 1956–1962.
Spence, P., Griffies, S. M., England, M. H., Hogg, A. M., Saenko, O. A., & Jourdain, N. C. (2014). Rapid subsurface warming and circulation changes of Antarctic coastal waters by poleward shifting winds. *Geophysical Research Letters*, *41*, 4601–4610. https://doi.org/10.1002/2014GL060613
St-Laurent, P., Klinck, J. M., & Dinniman, M. S. (2013). On the role of coastal troughs in the circulation of warm circumpolar deep water on Antarctic shelves. *Journal of Physical Oceanography*, *43*(1), 51–64.
Stewart, A. L., & Thompson, A. F. (2012). Sensitivity of the ocean's deep overturning circulation to easterly Antarctic winds. *Geophysical Research Letters*, *39*, L18604. https://doi.org/10.1029/2012GL053099
Stewart, A. L., & Thompson, A. F. (2013). Connecting Antarctic cross-slope exchange with Southern Ocean overturning. *Journal of Physical Oceanography*, *43*, 1453–1471.
Stewart, A. L., & Thompson, A. F. (2015a). The neutral density temporal residual mean overturning circulation. *Ocean Modelling*, *90*, 44–56.
Stewart, A. L., & Thompson, A. F. (2015b). Eddy-mediated transport of warm circumpolar deep water across the antarctic shelf break. *Geophysical Research Letters*, *42*, 432–440. https://doi.org/10.1002/2014GL062281
Stewart, A. L., & Thompson, A. F. (2016). Eddy generation and jet formation via dense water outflows across the Antarctic continental slope. *Journal of Physical Oceanography*, *46*(12), 3729–3750.
Su, Z., Stewart, A. L., & Thompson, A. F. (2014). An idealized model of Weddell Gyre export variability. *Journal of Physical Oceanography*, *44*(6), 1671–1688.
Thoma, M., Jenkins, A., Holland, D., & Jacobs, S. (2008). Modelling circumpolar deep water intrusions on the Amundsen Sea continental shelf, Antarctica. *Geophysical Research Letters*, *35*, L18602. https://doi.org/10.1029/2008GL034939
Thompson, A. F., Heywood, K. J., Schmidtko, S., & Stewart, A. L. (2014). Eddy transport as a key component of the Antarctic overturning circulation. *Nature Geoscience*, *7*(12), 879–884.
Wang, Q., Danilov, S., Fahrbach, E., Schröter, J., & Jung, T. (2012). On the impact of wind forcing on the seasonal variability of Weddell Sea Bottom Water transport. *Geophysical Research Letters*, *39*, L06603. https://doi.org/10.1029/2012GL051198
Wang, Q., Danilov, S., Hellmer, H., Sidorenko, D., Schroeter, J., & Jung, T. (2013). Enhanced cross-shelf exchange by tides in the western Ross Sea. *Geophysical Research Letters*, *40*, 5735–5739. https://doi.org/10.1002/2013GL058207
Whitworth, T., Orsi, A. H., Kim, S.-J., Nowlin, W. D., & Locarnini, R. A. (1998). Water masses and mixing near the Antarctic Slope Front. In *Ocean, ice, and atmosphere: Interactions at the Antarctic continental margin* (pp. 1–27). Washington, DC: American Geophysical Union.
Wolfe, C. L. (2014). Approximations to the ocean's residual circulation in arbitrary tracer coordinates. *Ocean Modelling*, *75*, 20–35.
Zhou, Q., Hattermann, T., Nøst, O. A., Biuw, M., Kovacs, K. M., & Lydersen, C. (2014). Wind-driven spreading of fresh surface water beneath ice shelves in the Eastern Weddell Sea. *Journal of Geophysical Research: Oceans*, *119*, 3818–3833. https://doi.org/10.1002/2013JC009556